SCIEPublish

Article

Lathyrus aphaca Extract MnO Nanoparticles: Synthesis, Characterization, and Photocatalytic Degradation of Methylene Blue Dye

Amir Hassan [1,*], Muhammad Haris [2], Sana Ullah Khan [2], Istikhar Khan [2], Muhammad Akif [2] and Naveed Akhtar [3]

[1] Faculty of Natural Sciences, Novosibirsk State University (NSU), 630090 Novosibirsk, Russia
[2] Department of Chemistry, Government Post Graduate College, Mardan 23200, Pakistan; muhammadharis23200@gmail.com (M.H.); chem.sanaullahkhan@gmail.com (S.U.K.); istikharkhan664@gmail.com (I.K.); akifm2155@gmail.com (M.A.)
[3] Department of Chemistry, Abdul Wali Khan University, Mardan 23200, Pakistan; naveedfarhad4@gmail.com

***** Corresponding author. E-mail: amirhassan741@gmail.com or a.khassan1@g.nsu.ru

Received: 20 March 2024; Accepted: 6 June 2024; Available online: 11 June 2024

ABSTRACT: Our environment has been impacted by man-made pollutants mainly industries make substantial use of synthetic dyes which exhibit cytotoxicity and have significant environmental consequences. Effective photocatalyst-based approaches for degrading synthetic dyes into less toxic chemical are of great interest. Synthesizing nanoparticles (NPs) using biological approaches, particularly plant-based approaches offer advantages, decreasing the risk of NPs losing biocompatibility during synthesis, cost-effectiveness, and eco-friendliness. In this study, we employed a green synthesis method to produce manganese oxide nanoparticles (MnO NPs) utilizing leaf extract from the *Lathyrus aphaca* plant. The synthesized MnOx NPs were characterized through various techniques; X-ray diffraction (XRD), scanning electron microscopy (SEM), energy-dispersive X-ray spectroscopy (EDX), Fourier-transform infrared spectroscopy (FTIR), and UV–visible spectroscopy. XRD analysis showed distinct peaks, indicated the presence crystallographic planes within the MnO_2 nanoparticles, thus confirming their crystalline structure. FTIR, showed the presence of the O-O stretching mode at a frequency of 719 cm^{-1}, the presence of MnO_6 oxides of manganese, and peak at 548 cm^{-1} corresponded to the Mn-O stretching mode. Furthermore, the green-synthesized manganese oxide nanoparticles exhibited promising photocatalytic and adsorption capabilities against Methylene Blue (MB) dye, leading to approximately 93% degradation of MB when treated with the green-synthesized MnO nanoparticles derived from plant extract. This highlights the efficacy and potential of these nanoparticles in environmental remediation applications, particularly in the degradation of methylene blue contaminants.

Keywords: *Lathyrus aphaca* extract; Green synthesis; Photocatalysis; Environmental remediation

1. Introduction

Our environment has been impacted by man-made pollutants from numerous manufacturing industries, such as rubber products, plastics, paper products, and leather goods. These manufacturing industries make substantial use of synthetic dyes such as methylene blue, Congo red, acid black 1, acid black 234, and acid black 210 [1,2]. These dyes exceed authorized limits and exhibit cytotoxicity. Repeated release of these dyes without proper removal or conversion into less dangerous compounds can have significant environmental consequences, ultimately affecting all living creatures [3–8]. Consequently, there is considerable interest in the search for simple, adaptable, and effective photocatalyst-based technologies for degrading synthetic dyes into less toxic chemical waste. Metal (Ag, Au, Pt, Cu, Zn, etc.) and the corresponding metal oxide (MgO, NiO, CuO, ZnO, TiO_2, etc.) nanoparticles (NPs) are considered promising materials due to their distinct physical properties, including a high surface area to volume ratio, regulated morphology, smaller dimensions, and light-absorbing properties [9–12]. These properties make them suitable for various applications, including biomedicine, biosensing, and optoelectronics. Metal and metal oxide NPs are extensively utilized in biomedicine due to their antibacterial, antimycotic, anticancer, antilarvicidal, and antidiabetic properties [9–12]. MnO NPs, in particular, have gained popularity in synthesis and manufacturing due to their reduced toxicity [13]. Nanoparticles are

https://doi.org/10.35534/prp.2024.10004

typically synthesized using chemical and physical methods, both of which are energy-intensive, involve hazardous chemicals for reduction and capping, and are difficult to scale. The use of harmful chemicals compromises the biocompatibility of NPs, as these compounds may remain on the NPs surface even after multiple washings, limiting their use in biological applications [14,15]. Therefore, synthesizing NPs using biological approaches, particularly plant-based methodologies, serves as an alternative to traditional methods. Plant-based biological approaches offer several advantages, including one-pot synthesis, robustness, cost-effectiveness, and eco-friendliness. The biological molecules present in plants act as reduction and capping agents, decreasing the risk of NPs losing biocompatibility during synthesis [6–8]. Moreover, the use of plant-based methods is considered safe and environmentally friendly. In our current research study, we synthesized manganese oxide nanoparticles (MnO NPs) utilizing an innovative approach involving the leaf extract of *Lathyrus aphaca*. *Lathyrus aphaca*, renowned for its medicinal properties, has historically been employed in the treatment of various diseases. In this investigation, we have examined the MnO NPs with the *Lathyrus aphaca*, which acted as a reducing and stabilizing agent. Subsequently, the synthesized MnO NPs were tested to evaluate their efficacy as a photocatalyst against methylene blue.

2. Materials and Methods

All chemicals utilized in the experiment, including $MnSO_4 \cdot H_2O$, NaOH, methylene blue dye, ethanol, methanol, and distilled water, were of analytical grade and were employed without additional purification.

2.1. Plant Extraction

Approximately 50 g of dried and ground plant sample is placed in a sealed Pyrex glass jar, to which 400 mL of absolute methanol is added. The jar is left undisturbed for up to 3 weeks at room temperature, with daily agitation to facilitate the release of plant-soluble phytochemicals. The resulting soaked extract is filtered using a standard filter paper (Whatman filter paper) to obtain a concentrated methanolic extract through solvent evaporation. Subsequently, the extract is further concentrated to achieve the desired dry extract for subsequent processing [16–20].

2.2. Synthesis of MnOx NPs

A 100 mL solution of 0.1 M $MnSO_4 \cdot H_2O$ was placed into a 500 mL beaker, followed by the addition of 100 mL of plant extract were carried based on literature [21,22]. Subsequently, a 0.1 M NaOH solution was carefully added dropwise to the beaker while stirring constantly for approximately 1 h at a pH of 8.0 and a temperature of 50 °C. Afterward, the mixture was filtered and washed with methanol to eliminate impurities. The resulting precipitates were then dried in an oven at 90 °C for 1 h before being subjected to calcination in a muffle furnace at 150 °C for 2 h. These materials were subsequently utilized for further characterization and the photocatalytic degradation of methylene blue dye.

2.3. Photocatalytic Degradation of MnO NPs

The photocatalytic degradation activity of green-synthesized MnO nanoparticles was assessed using methylene blue dye as a model system, adopted from [23,24]. Initially, 0.05 g of green-synthesized MnO nanoparticles were introduced into 100 mL of methylene blue dye solution and the resulting suspension was left in a dark for about 1 h to achieve adsorption-desorption equilibrium. Subsequently, the suspensions were exposed to solar irradiation without external pressure or pH adjustment, with the temperature maintained at 30 °C. Throughout the irradiation process, continuous stirring was maintained using a magnetic stirrer to ensure uniform mixing. At regular intervals (every 20 minutes for 2 h), 5 mL samples were withdrawn for analysis. These samples were centrifuged to separate the photocatalyst (MnO nanoparticles), and the remaining dye content was determined using a UV spectrophotometer at the specific absorption peak (664 nm) of methylene blue. The percentage degradation of the dye under solar light exposure was calculated using the Equation (1):

$$\% D = \frac{C_o - C_t}{C_o} \times 100 \quad (1)$$

where C_o is the initial dye concentration and C_t is the dye concentration at time t in min.

A UV light box was used to carry out all of the photochemical processes. The wavelength distribution of the emission ranged from 200 to 800 nm. The lamp was placed approximately 10 cm away from the dye suspension. The dye concentration was monitored using a spectrophotometer (UV-1601, Shimadzu, Japan). Three consecutive

experiments were carried out under sunlight irradiation to assess the recovery and stability of MnO nanoparticles as a photocatalyst. Following each run, the MnO nanoparticles photocatalyst was extracted, cleaned with deionized water and ethanol, dried, and subsequently reused. The degradation efficiency of the nanoparticles was then evaluated.

2.4. Characterization

The green-synthesized MnO nanoparticles were then characterized using various spectroscopic techniques. The band gap energy was determined by employing the absorption spectra of a UV-Visible spectrophotometer. X-ray diffraction (XRD) analysis was performed to detect the crystalline structure of the synthesized nanoparticles. Energy-dispersive X-ray spectroscopy (EDX) analysis was conducted to confirm the chemical composition of the green-synthesized MnO nanoparticles. Morphology determination of the synthesized nanoparticles was carried out using a scanning electron microscope (SEM). Fourier transform infrared (FTIR) analysis of the synthesized nanoparticles was performed to highlight the involvement of biological moieties from the plant extract.

3. Results and Discussion

3.1. X-ray Diffraction Analysis

The X-ray diffraction (XRD) pattern depicted in [Figure 1] illustrates the analysis of manganese oxide (MnO) nanoparticles synthesized through a green method. The XRD pattern closely aligns with existing literature, revealing distinct diffraction peaks at specific angles corresponding to crystal planes. These angles are recorded as follows: (6.4°, 10.24°, 14.88°, 18.66°, 26.22°, 29.22°, 36.14°, 38.72°, 44.18°, 47.18°, 49.92°, 53.24°, 62.44°, and 71.32°). Notably, the peaks of greatest prominence emerge at approximately 10.24°, 18.66°, 26.22°, 47.18°, and 62.44°. These prominent peaks signify the presence of specific crystallographic planes within the MnO_2 nanoparticles, showing their crystalline nature. The synthesis process involves utilizing plant extract as a dual agent for both reduction and oxidation. The resultant XRD pattern confirms the crystallinity of the synthesized nanoparticles. Moreover, the synthesized nanoparticles exhibit heightened peak intensity and sharpness, indicative of their extremely crystalline nature. Any observed impurity peaks within the XRD pattern are minimal, further affirming the purity of the synthesized MnO nanoparticles. The XRD graph refinement was performed, and the *hkl* Miller indices were assigned based on the literature. Manjula et al. [25] assigned their XRD patterns to a tetragonal phase and compared them with standard data from the JCPDS card (File no: 14-644). They proposed that the synthesized MnO_2 nanoparticles are of poor crystalline nature, hence the diffraction peaks are indexed as a tetragonal phase [26]. No additional diffraction peaks related to impurities were detected, indicating the good quality of the synthesized MnO_2 [27]. While, Zheng et al. [28] found that their XRD reflections readily indexed to cubic MnO with a lattice constant of 4.443 Å, in good accordance with the literature (JCPDS 89–4835). They observed no other phases of manganese oxide, indicating the monophase of cubic MnO. Similarly, Mansoor et al. [29] revealed that the synthesized MnO nanoparticles exhibited a good crystalline nature with a wurtzite hexagonal structure, consistent with the JCPDS card number (01-075-1533) [30].

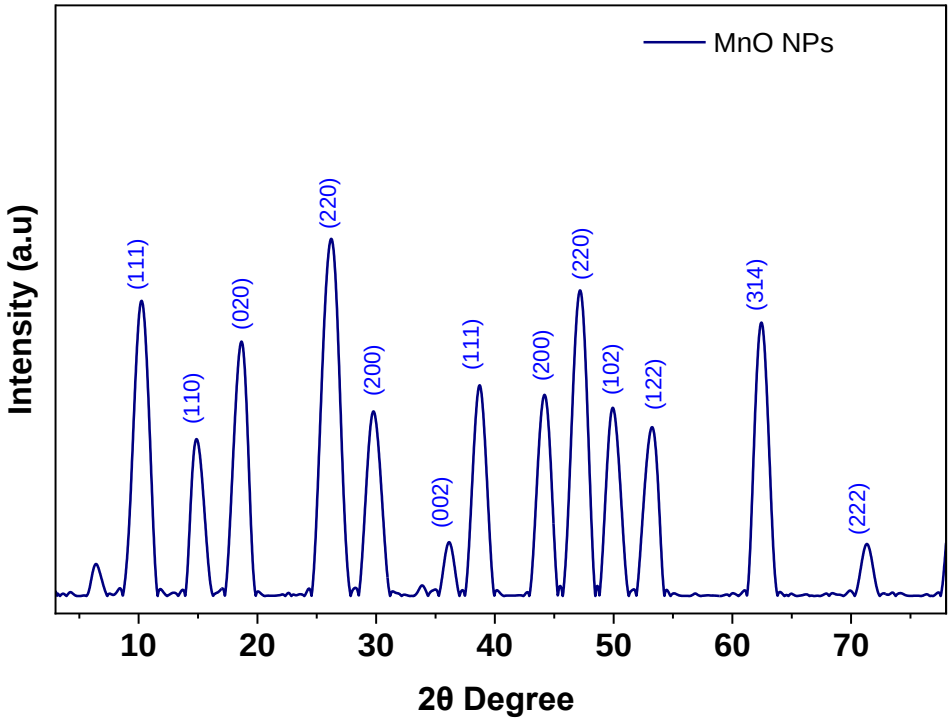

Figure 1. XRD pattern of plant extracted MnOx NPs.

3.2. SEM and EDX Analysis

The size and shape of manganese oxide (MnO) nanoparticles extracted from green plants were studied using a scanning electron microscope (SEM). The nanoparticles were examined within a range of 20 micrometers, using an electron beam accelerated to 50 kilovolts. The SEM images, shown in [Figure 2], revealed the morphology and average size of the nanoparticles. The analysis confirmed successful synthesis of MnO nanoparticles, which had sizes in the nanometer range. The particles appeared randomly arranged and asymmetrical, with closely spaced arrangements. [Figure 2] showed zoomed-in views of the nanoparticles, indicating an average size of approximately $\geq \pm$ 50–70 nanometers, with clear boundaries visible upon further magnification. However, SEM scans indicated that the produced MnO nanoparticles were dispersed randomly. EDX analysis was employed to examine the formation and chemical composition of manganese oxide (MnO) nanoparticles synthesized from green sources. The presence of elemental manganese (Mn) in the samples was confirmed through EDX analysis, as showed in [Figure 3], showcasing the EDX pattern and mapping. This verification underscores the effective synthesis of nanoparticles using biological components extracted from *Lathyrus aphaca* leaf extract.

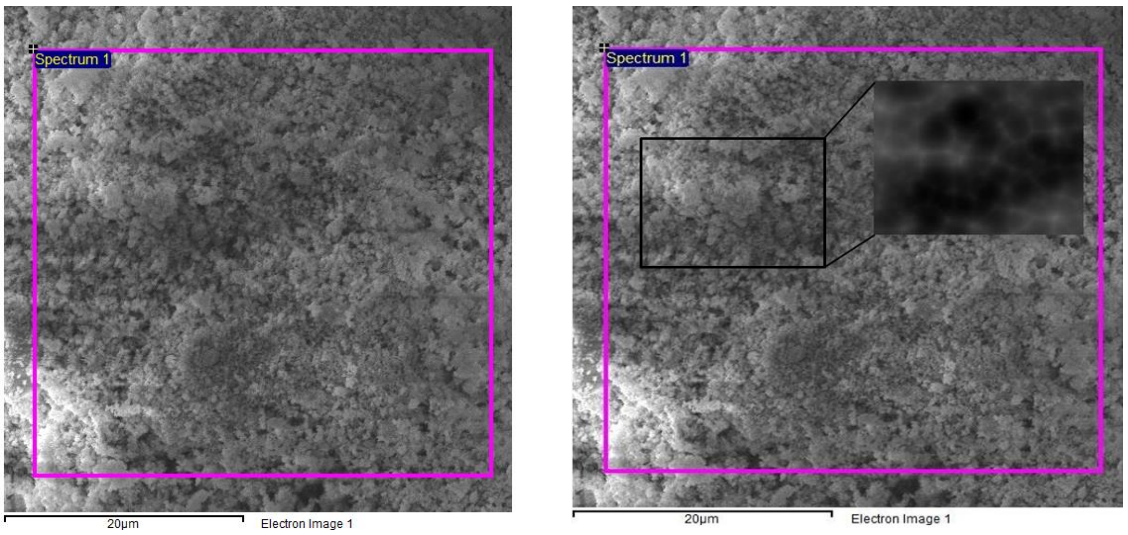

Figure 2. Scanning electron microscopy images of MnO NPs.

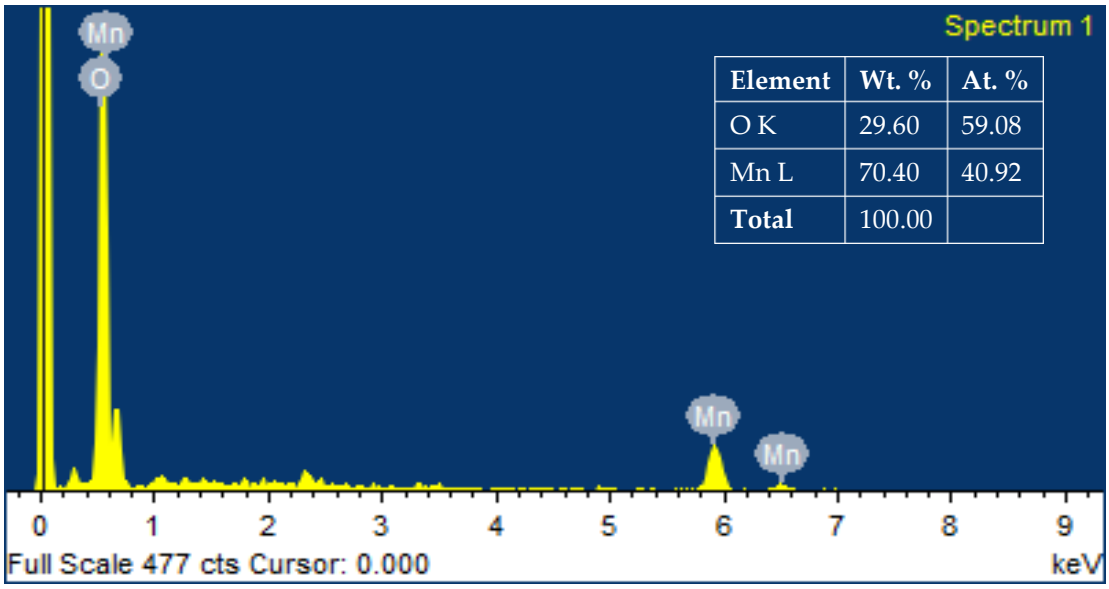

Figure 3. EDX spectrum plant extracted MnOx NPs.

EDX peaks in the spectrum indicated the presence of Mn at lower energy levels (around 1 kilo electron volts, keV) with the highest peak representing MnO, and at higher energy levels (above 5 keV) representing elemental manganese. Furthermore, peaks corresponding to oxygen (O) were observed, confirming the adsorption of biological molecules from the plant extract onto the nanoparticle surfaces. The presence of oxygen confirms the oxide form of the Mn nanoparticles. The absence of impurities and the high concentration of Mn were confirmed by the EDX analysis. Consequently, it can be inferred that the desired nanoparticles were successfully synthesized using plant leaf extract. [Figure 3] presents the observed atomic percentages for all elements, with Mn accounting for 70.40% and O for 29.60% by weight. The EDX pattern of the green-synthesized MnO nanoparticles was consistent with previously published literature [23,26–33]. The UV-visible graph, depicted as [Figure 4], illustrates significant optical properties of the synthesized nanoparticles and their interaction with ultraviolet (UV) and visible light. This graph provides insights into the absorbance and reflection characteristics of the nanoparticles across different wavelengths. UV-visible spectroscopy is instrumental in identifying the electronic transitions of nanoparticles and assessing their potential applications, including catalytic activity. Additionally, the X-ray diffraction (XRD) profile reveals distinct peaks characteristic of the synthesized nanoparticles, which align precisely with data from existing literature. This confirms the structural properties of the nanoparticles as consistent with the literature data [25,33–37].

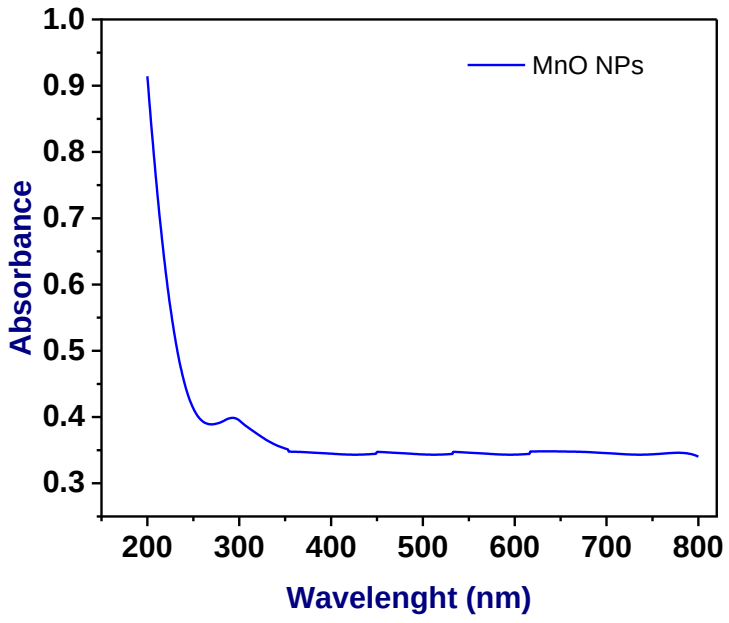

Figure 4. UV–visible graph of the green synthesized MnOx nanoparticles.

3.3. FTIR Analysis

Fourier Transform Infrared (FTIR) spectroscopy is essential for the identification of chemical functional groups and the characterization of intermolecular forces resulting from the interaction between two or more mixtures of different functional groups or compounds. In this study, FTIR analysis was employed, as showed in [Figure 5]. Plants contain a variety of phytochemicals, constituting a rich source of various functional groups. Consequently, FTIR analysis holds promise in predicting the presence of additional functional groups containing heteroatoms, predominantly involving carbon bonded with H, O, N, OH, and X, when compared to manganese oxide synthesized nanoparticles. Through extensive review of the literature [38–44], manganese oxide nanoparticles (MnO NPs) were examined using FTIR analysis within the frequency range of 719.80 to 494.81 cm^{-1}.

Our findings, illustrated in [Figure 5], revealed the presence of the O-O stretching mode at a frequency of 719 cm^{-1}, and showed the presence of MnO_6 oxides of manganese. Furthermore, a peak observed at 548 cm^{-1} corresponded to the Mn-O stretching mode, aligning closely with existing literature [45–47]. Consequently, these findings suggest that the green-synthesized MnO NPs are coated with biologically active molecules derived from plant leaf extracts, encompassing diverse functional groups. The peaks observed at wavenumbers above 3400 cm^{-1} correspond to the stretching vibrations of hydroxyl groups OH, while the peak around 1720 cm^{-1} is associated with the stretching vibration of carbonyl groups CO showed carbonyl and other carbon functional groups. These peaks indicate the presence of O containing functional groups attached to the carbon structure. The Fourier-transform infrared (FTIR) spectra also reveal the presence of other fundamental functional groups commonly found in plant-derived nanoparticles, as illustrated in [Figure 5].

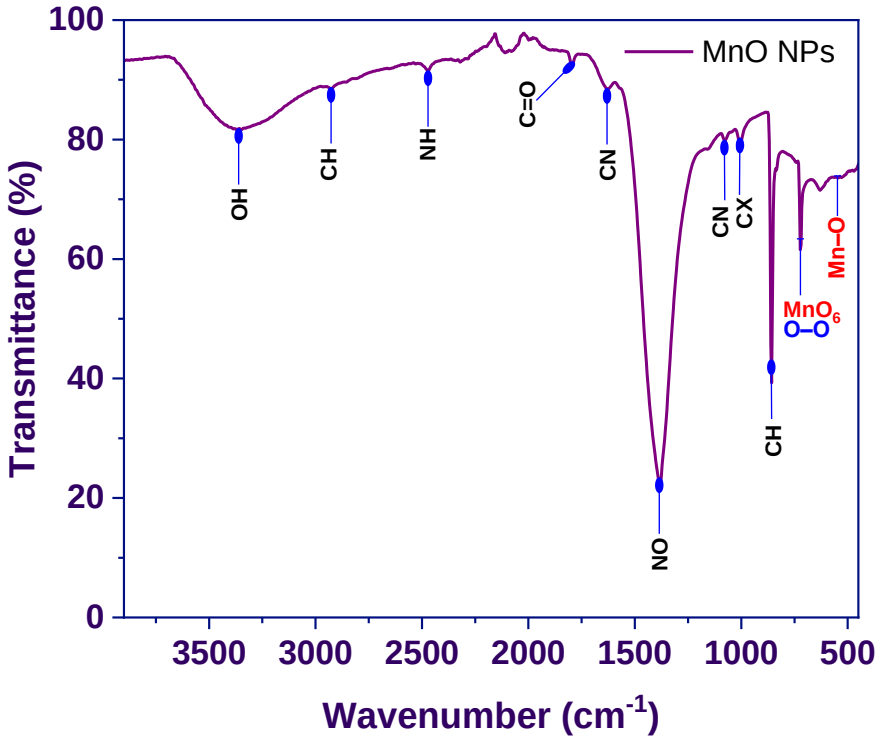

Figure 5. FTIR pattern of the green synthesized MnOx nanoparticles.

3.4. Photocatalytic Degradation of Methylene Blue (MB) Dye

We have examined the photocatalytic degradation of methylene blue (MB) dye employing green-synthesized manganese oxide nanoparticles (MnO NPs) under ultraviolet (UV) light irradiation as illustrated in [Figure 6]. The experimental setup utilized a UV lamp as the radiation source. Initially, the self-degradation behavior of MB dye was assessed in the absence of synthetized photocatalyst (MnO NPs), yielding no detection of self-degradation [44–47]. Subsequently, the photocatalytic activity of green-synthesized MnO NPs was evaluated, demonstrating efficient degradation of MB dye under UV light irradiation for duration of 120 minutes and noted that the observed photocatalytic activity corresponds to the average efficiency within the UV lamp irradiation spectrum. Furthermore [Figure 7] illustrates the percentage degradation of methylene blue (MB) over time. A single sample with a concentration of 40 parts per million

(ppm) was employed in the experiment. The results indicate a clear direct correlation between time and the percentage degradation of methylene blue dye. At a maximum duration of 120 min, MB experienced approximately 93% degradation when treated with green synthesized plant extracted MnO nanoparticles. This underscores the efficiency and potential of the synthesized nanoparticles in degrading methylene blue. In our analysis, the process of catalytic degradation of MB follows the pseudo-first-order kinetic model. We conducted both linear and non-linear fitting of the curve, as illustrated in Figure 8.

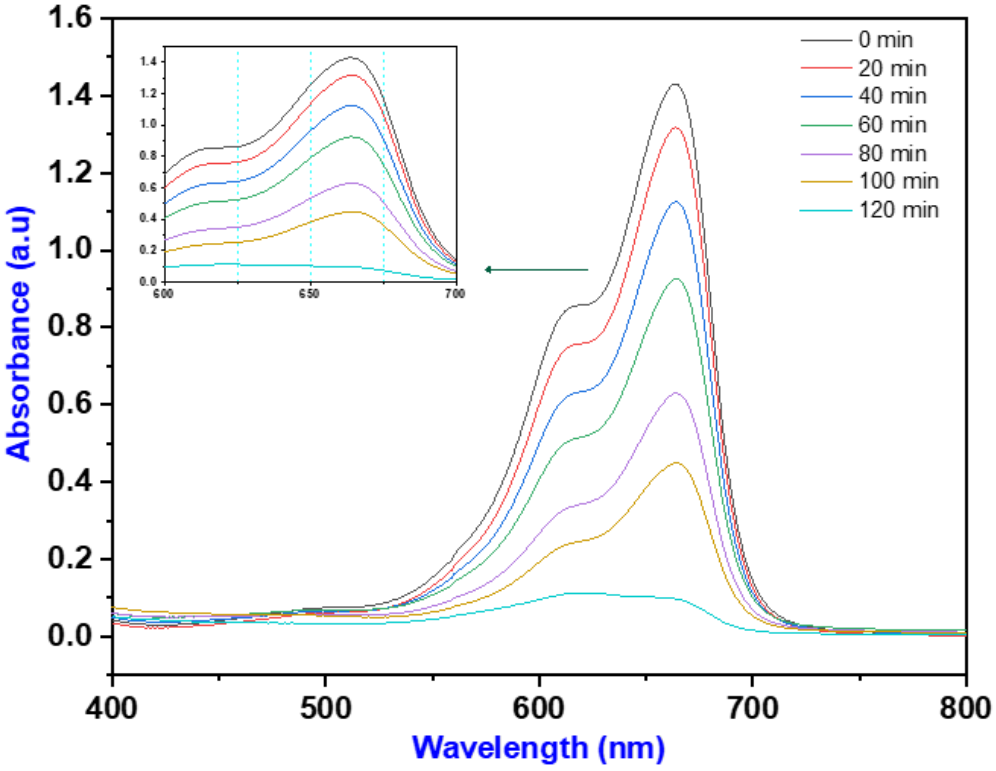

Figure 6. MB degradation analysis under UV by MnOx nanoparticles.

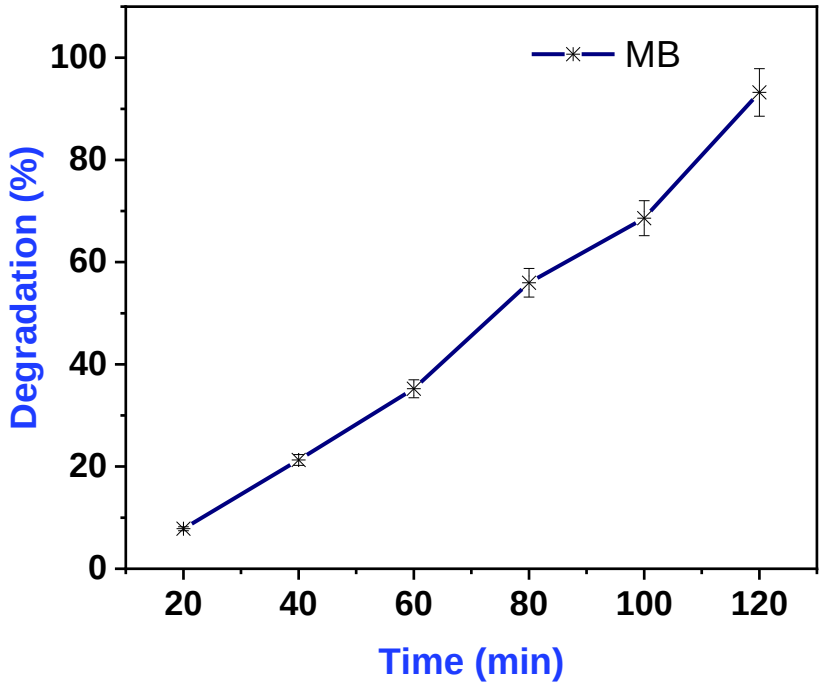

Figure 7. Percent degradation of methylene blue dye by green synthesized MnOx NPs.

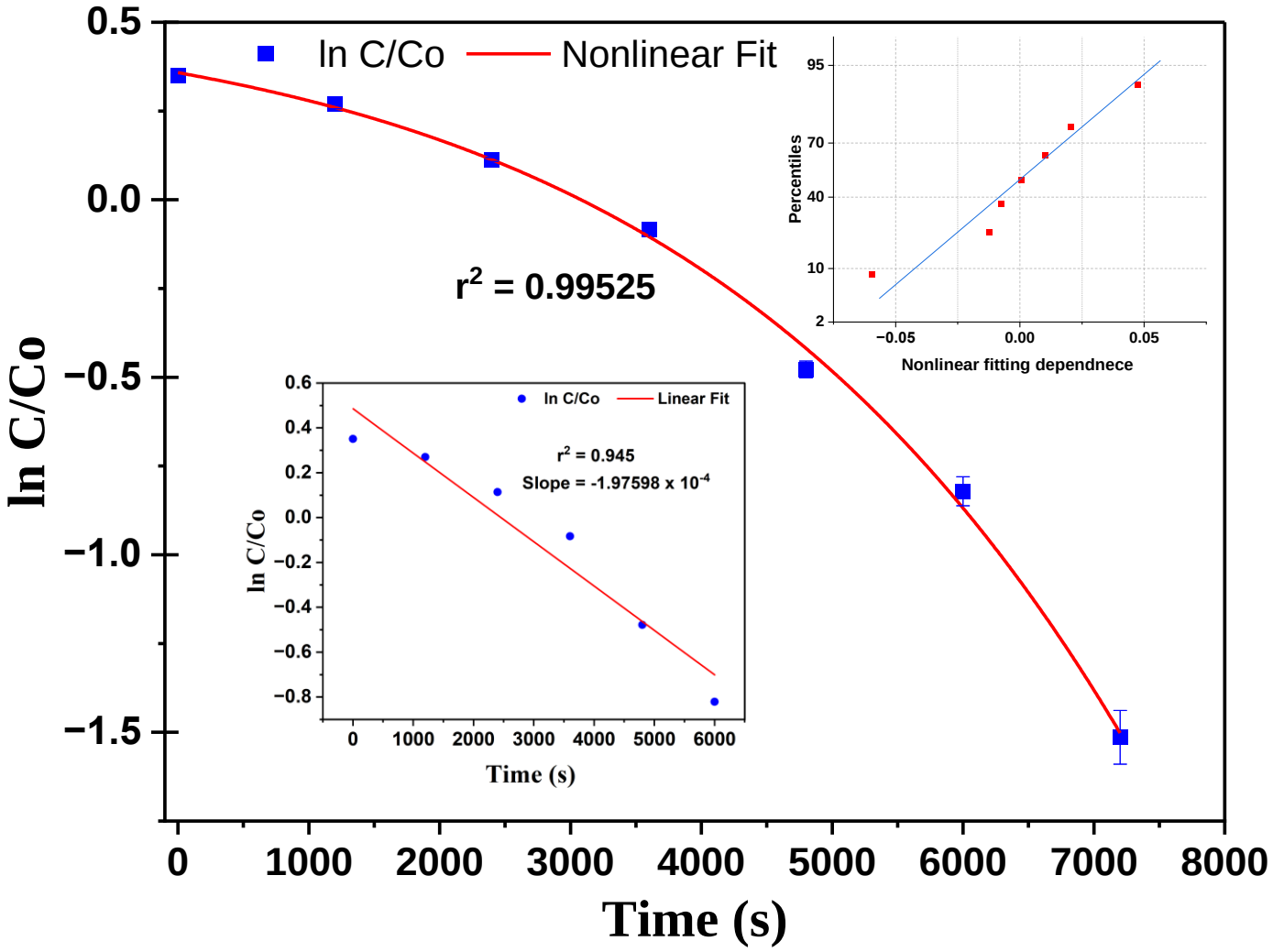

Figure 8. Pseudo-first order kinetic model followed by MnOx nanoparticles MB degradation.

Table 1 provides a comprehensive analysis of the efficacy of the MB dye removal between MnOx NPs synthesized utilizing *Lathyrus aphaca* extract with other environmentally friendly synthesized NPs [22,48–54]. The current study reveals that the MnOx NPs employed exhibit superior performance compared to the relevant literature. *Lathyrus aphaca* extract MnOx NPs demonstrate efficient ability to remove dye at maximum concentrations, requiring minimal time and concentration. Remarkably, this superior performance is achieved without the reaction environment control parameters such as temperature and pH. This underscores the promising potential of MnOx NPs synthesized with *Lathyrus aphaca* extract for robust and efficient dye removal applications.

Table 1. Comparative analysis of green-synthesized NPS and their efficacy against Methylene Blue.

S. No.	NPs	Degradation Method	Concentration	Removal Efficiency	Time (min)	Ref.
1	Fe_2O_3	Photocatalytic	15 mg in 100 mL	98%	59	[48]
2	Fe oxide	Photocatalytic	0.8 g/L	76.6%	360	[49]
3	IONPs	Catalytic in presence of H_2O_2	10 mg in 8 mL	98.6%	360	[50]
4	MIO NPs	Photocatalyst	30 mg in 50 mL	99%	110	[51]
5	FeOx NPs	Photocatalyst	-	80%	150	[52]
6	FOx NP	Catalytic in presence of $NaBH_4$	15 mg in 3 mL	99%	220	[53]
7	IOx NPs	Catalytic in presence of $NaBH_4$	2 mg in 3 mL	80%	30	[54]
8	AI-MnO NPs	Photocatalytic	0.05 g/100 mL	31%	180	[22]
9	MnO NPS	Photocatalytic	0.5 mg/1 mL	93%	120	Present

4. Conclusions

In this investigation, we employed a green synthesis method to produce manganese oxide nanoparticles (MnO NPs) for the first time, utilizing leaf extract from the *Lathyrus aphaca* plant. Our findings of FTIR, revealed the presence of the O-O stretching mode at a frequency of 719 cm^{-1}, and showed the presence of MnO_6 oxides of manganese, and peak observed at 548 cm^{-1} corresponded to the Mn-O stretching mode, aligning closely with existing literature. Furthermore, the green-synthesized manganese oxide nanoparticles exhibited promising photocatalytic and adsorption capabilities against Methylene Blue (MB) dye, leading to approximately 93% degradation of MB when treated with the green-synthesized MnO nanoparticles derived from plant extract. This highlights the efficacy and potential of these nanoparticles in environmental remediation applications, particularly in the degradation of methylene blue contaminants.

Acknowledgments

The author acknowledges the affiliated institute for providing research facilities and financial support for conducting research and publication support.

Author Contributions

M.H. and S.U.K. are credited for experimental and characterization work, A.H. for reviewing, writing, and submission, while I.K., M.A. and N.A. contributed to the relevant literature. All authors have read the manuscript and agreed to its submission.

Ethics Statement

Not applicable.

Informed Consent Statement

Not applicable.

Funding

Financial support provided by institutional affiliations.

Declaration of Competing Interest

The authors declare no conflicts of interest.

References

1. Khan SA, Arshad Z, Shahid S, Arshad I, Rizwan K, Sher M, et al. Synthesis of TiO_2/Graphene oxide nanocomposites for their enhanced photocatalytic activity against methylene blue dye and ciprofloxacin. *Compos. Part B Eng.* **2019**, *175*, 107120.
2. Abbasi A, Sajadi SMS, Amiri O, Hamadanian M, Moayedi H, Salavati-Niasari M, er al. $MgCr_2O_4$ and $MgCr_2O_4$/Ag nanostructures: Facile size-controlled synthesis and their photocatalytic performance for destruction of organic contaminants. *Compos. Part B Eng.* **2019**, *175*, 107077.
3. Hirpara DG, Gajera HP. Green synthesis and antifungal mechanism of silver nanoparticles derived from chitin-induced exometabolites of Trichoderma interfusant. *Appl. Organomet. Chem.* **2020**, *34*, e5407.
4. Zangeneh MM, Zangeneh A. Novel green synthesis of Hibiscus sabdariffa flower extract conjugated gold nanoparticles with excellent anti-acute myeloid leukemia effect in comparison to daunorubicin in a leukemic rodent model. *Appl. Organomet. Chem.* **2020**, *34*, e5271.
5. Al-Radadi NS. Green synthesis of platinum nanoparticles using Saudi's Dates extract and their usage on the cancer cell treatment. *Arab. J. Chem.* **2019**, *12*, 330–349.
6. Tahvilian R, Zangeneh MM, Falahi H, Sadrjavadi K, Jalalvand AR, Zangeneh, A. Green synthesis and chemical characterization of copper nanoparticles using Allium saralicum leaves and assessment of their cytotoxicity, antioxidant, antimicrobial, and cutaneous wound healing properties. *Appl. Organomet. Chem.* **2019**, *33*, e5234.
7. Mahdavi B, Saneei S, Qorbani M, Zhaleh M, Zangeneh A, Zangeneh MM, et al. Ziziphora clinopodioides Lam leaves aqueous extract mediated synthesis of zinc nanoparticles and their antibacterial, antifungal, cytotoxicity, antioxidant, and cutaneous wound healing properties under in vitro and in vivo conditions. *Appl. Organomet. Chem.* **2019**, *33*, e5164.

8. Baharfar R, Zareyee, D, Allahgholipour SL. Synthesis and characterization of MgO nanoparticles supported on ionic liquid-based periodic mesoporous organosilica (MgO@ PMO-IL) as a highly efficient and reusable nanocatalyst for the synthesis of novel spirooxindole-furan derivatives. *Appl. Organomet. Chem.* **2019**, *33*, e4805.
9. Iqbal J, Abbasi BA, Mahmood T, Hameed S, Munir A, Kanwal, S. Green synthesis and characterizations of Nickel oxide nanoparticles using leaf extract of Rhamnus virgata and their potential biological applications. *Appl. Organomet. Chem.* **2019**, *33*, e4950.
10. Ijaz F, Shahid S, Khan SA, Ahmad, W, Zaman, S. Green synthesis of copper oxide nanoparticles using Abutilon indicum leaf extract: Antimicrobial, antioxidant and photocatalytic dye degradation activitie. *Trop. J. Pharm. Res.* **2017**, *16*, 743–753.
11. Khan SA, Noreen F, Kanwal S, Iqbal, A, Hussain, G. Green synthesis of ZnO and Cu-doped ZnO nanoparticles from leaf extracts of Abutilon indicum, Clerodendrum infortunatum, Clerodendrum inerme and investigation of their biological and photocatalytic activities. *Mater. Sci. Eng. C* **2018**, *82*, 46–59.
12. Haq S, Rehman W, Waseem M, Shah A, Khan AR, Rehman MU, et al. Green synthesis and characterization of tin dioxide nanoparticles for photocatalytic and antimicrobial studies. *Mater. Res. Express* **2020**, *7*, 025012.
13. Veeramani H, Aruguete D, Monsegue N, Murayama M, Dippon U, Kappler, A, et al. Low-temperature green synthesis of multivalent manganese oxide nanowires. *ACS Sustain. Chem. Eng.***2013**, *1*, 1070–1074.
14. Khan SA, Kanwal S, Rizwan, K, Shahid, S. Enhanced antimicrobial, antioxidant, in vivo antitumor and in vitro anticancer effects against breast cancer cell line by green synthesized un-doped SnO_2 and Co-doped SnO_2 nanoparticles from Clerodendrum inerme. *Microb. Pathog.* 2**018**, *125*, 366–384.
15. Shahid S, Fatima U, Sajjad, R, Khan SA. Bioinspired nanotheranostic agent: Zinc oxide; green synthesis and biomedical potential. *Dig. J. Nanomater. Biostruct.* **2019**, *14*, 1023–1031.
16. Hassan A, Mohmand NZK, Ullah H, Shah Y. Rumax dentatus Synthesis of Silver Nanoparticles, Antimicrobial Activity and Characterization. *J. Sib. Fed. Univ. Chem.* **2023**, *16*, 180–190.
17. Hassan A, Khan Mohmand NZ, Ullah H, Hussain A. Antioxidant, antidiabetic, and antihypertension inhibitory potentials of phenolic rich medicinal plants. *J. Chem.* **2022**, *2022*, 9046780.
18. Hassan A, Ullah I, Ahmad W. Isolation and Evaluation of Antibacterial Potential Test of Plant Carthamus oxycantha. *J. Trop. Pharm. Chem.* **2021**, *5*, 299–308.
19. Amir H, Shahzeb MW, Nawaz, K. Extraction and antibacterial potential of traditional medicinal plant Cypreus compressus. *TMR Mod. Herb. Med.* **2021**, *4*, 22.
20. Hassan A, Ullah H, Israr M. The antioxidant activity and phytochemical analysis of medicinal plant Veronica biloba. *Lett. Appl. NanoBioSci*. **2019**, *8*, 732–738.
21. Singh H, Du J, Singh P, Yi TH. Ecofriendly synthesis of silver and gold nanoparticles by Euphrasia officinalis leaf extract and its biomedical applications. *Artif. Cells Nanomed. Biotechnol.* **2018**, *46*, 1163–1170.
22. Khan SA, Shahid S, Shahid B, Fatima U, Abbasi SA. Green synthesis of MnO nanoparticles using abutilon indicum leaf extract for biological, photocatalytic, and adsorption activities. *Biomolecules* **2020**, *10*, 785.
23. Mansoor S, Nabi GAK, Hussain S, Javid Z, Jan FA. Synthesis, Characterization, Kinetic and Thermodynamic Study of Photocatalytic Degradation of Malachite Green Dye Using MnO_2 Nanoparticles as Catalyst. *Chem. Afr.* **2024**, *7*, 1575–1583.
24. Faisal S, Jan FA, Saleem S, Ullah R, Wajidullah, Ullah, N, et al. Mediated synthesis of cobalt oxide and zinc-doped cobalt oxide nanoparticles: Characterization and evaluation for environmental, antibacterial and cytotoxic potential. *Nanotechnol. Environ. Eng.* **2022**, *7*, 675–689.
25. Manjula R, Thenmozhi M, Thilagavathi S, Srinivasan R, Kathirvel A. Green synthesis and characterization of manganese oxide nanoparticles from Gardenia resinifera leaves. *Mater. Today Proc.* **2020**, *26*, 3559–3563.
26. Ahmed S, Hasan MM. Exploring globally used antiurolithiatic plants of M to R families: Including Myrtaceae, Phyllanthaceae, Piperaceae, Polygonaceae, Rubiaceae and Rutaceae. *J. Pharmacogn. Phytochem.* **2017**, *6*, 325–335.
27. Zhang Y, Yan Y, Wang X, Li G, Deng D, Jiang, L, et al. Facile synthesis of porous Mn_2O_3 nanoplates and their electrochemical behavior as anode materials for lithium ion batteries. *Chem. –A Eur. J.* **2014**, *20*, 6126–6130.
28. Zheng M, Zhang H, Gong X, Xu R, Xiao Y, Dong H, et al. A simple additive-free approach for the synthesis of uniform manganese monoxide nanorods with large specific surface area. *Nanoscale Res. Lett.* **2013**, *8*, 1–7.
29. Labhane PK, Sonawane GH, Sonawane SH. Influence of rare-earth metal on the zinc oxide nanostructures: Application in the photocatalytic degradation of methylene blue and p-nitro phenol. *Green Process. Synth.* **2018**, *7*, 360–371.
30. Jaganyi D, Altaf M, Wekesa I. Synthesis and characterization of whisker-shaped MnO_2 nanostructure at room temperature. *Appl. Nanosci.* **2013**, *3*, 329–333.
31. Wang HQ, Yang GF, Li QY, Zhong XX, Wang FP, Li ZS, et al. Porous nano-MnO_2: Large scale synthesis via a facile quick-redox procedure and application in a supercapacitor. *New J. Chem.* **2011**, *35*, 469–475.

32. Moon SA, Salunke BK, Alkotaini B, Sathiyamoorthi E, Kim BS. Biological synthesis of manganese dioxide nanoparticles by Kalopanax pictus plant extract. *IET Nanobiotechnol.* **2015**, *9*, 220–225.
33. Chatterjee S, Ja A, Subramanian A, Subramanian SA. Synthesis and characterization of manganese dioxide using brassica oleracea (cabbage). *J. Ind. Pollut. Control* **2017**, *33*, 1627–1632.
34. Rajabathar JR, Al-lohedan HA, Arunachalam P, Issa ZA, Gnanamani MK, Appaturi JN, et al. Synthesis and characterization of metal chalcogenide modified graphene oxide sandwiched manganese oxide nanofibers on nickel foam electrodes for high performance supercapacitor applications. *J. Alloys Compd.* **2021**, *850*, 156346.
35. Li Y, Wang J, Zhang Y, Banis MN, Liu J, Geng D, et al. Facile controlled synthesis and growth mechanisms of flower-like and tubular MnO_2 nanostructures by microwave-assisted hydrothermal method. *J. Colloid Interface Sci.* **2012**, *369*, 123–128.
36. Guan L, Yu L, Chen GZ. Capacitive and non-capacitive faradaic charge storage. *Electrochim. Acta* **2016**, *206*, 464–478.
37. Ensafi AA, Ahmadi N, Rezaei, B. Electrochemical preparation and characterization of a polypyrrole/nickel-cobalt hexacyanoferrate nanocomposite for supercapacitor applications. *RSC Adv.* 2**015**, *5*, 91448–91456.
38. Ouda E, Yousf N, Magar HS, Hassan RY, Duraia ESM. Electrochemical properties of MnO_2-based carbon nanomaterials for energy storage and electrochemical sensing. *J. Mater.Sci. Mater. Electron.* **2023**, *34*, 731.
39. Chen H, Dong X, Shi J, Zhao J, Hua Z, Gao J, et al. Templated synthesis of hierarchically porous manganese oxide with a crystalline nanorod framework and its high electrochemical performance. *J. Mater. Chem.* **2007**, *17*, 855–860.
40. Chen H, He J. Facile synthesis of monodisperse manganese oxide nanostructures and their application in water treatment. *J. Phys. Chem. C* **2008**, *112*, 17540–17545.
41. Estelrich J, Sánchez-Martín MJ, Busquets MA. Nanoparticles in magnetic resonance imaging: From simple to dual contrast agents. *Int. J. Nanomed.* **2015**, *10*, 1727–1741.
42. Zheng M, Liu Y, Jiang K, Xiao Y, Yuan, D. Alcohol-assisted hydrothermal carbonization to fabricate spheroidal carbons with a tunable shape and aspect ratio. *Carbon* **2010**, *48*, 1224–1233.
43. Sevilla, M, Fuertes AB. Chemical and structural properties of carbonaceous products obtained by hydrothermal carbonization of saccharides. *Chem. –A Eur. J.* **2009**, *15*, 4195–4203.
44. Carmona-Carmona AJ, Mora ES, Flores JIP, Márquez-Beltrán C, Castañeda-Antonio MD, González-Reyna MA, et al. Photocatalytic Degradation of Methylene Blue by Magnetic Opal/Fe_3O_4 Colloidal Crystals under Visible Light Irradiation. *Photochem* **2023**, *3*, 390–407.
45. Zhang J, Li B, Yang W, Liu J. Synthesis of magnetic Fe_3O_4@ hierarchical hollow silica nanospheres for efficient removal of methylene blue from aqueous solutions. *Ind. Eng. Chem. Res.* **2014**, *53*, 10629–10636.
46. Vinothkannan M, Karthikeyan C, Kim AR, Yoo DJ. One-pot green synthesis of reduced graphene oxide (RGO)/Fe_3O_4 nanocomposites and its catalytic activity toward methylene blue dye degradation. *Spectrochim. Acta Part A Mol. Biomol. Spectrosc.* **2015**, *136*, 256–264.
47. Jaast, S, Grewal A. Green synthesis of silver nanoparticles, characterization and evaluation of their photocatalytic dye degradation activity. *Curr. Res. Green Sustain. Chem.* **2021**, *4*, 100195.
48. Bibi I, Nazar N, Ata S, Sultan M, Ali A, Abbas A, et al. Green synthesis of iron oxide nanoparticles using pomegranate seeds extract and photocatalytic activity evaluation for the degradation of textile dye. *J. Mater. Res. Technol.* **2019**, *8*, 6115–6124.
49. Bhuiyan MSH, Miah MY, Paul SC, Aka TD, Saha O, Rahaman MM, et al. Green synthesis of iron oxide nanoparticle using Carica papaya leaf extract: Application for photocatalytic degradation of remazol yellow RR dye and antibacterial activity. *Heliyon* **2020**, *6*, e04603.
50. Kouhbanani MAJ, Beheshtkhoo N, Amani AM, Taghizadeh S, Beigi V, Bazmandeh AZ, et al. Green synthesis of iron oxide nanoparticles using Artemisia vulgaris leaf extract and their application as a heterogeneous Fenton-like catalyst for the degradation of methyl orange. *Mater. Res. Express* **2018**, *5*, 115013.
51. Bishnoi S, Kumar A, Selvaraj, R. Facile synthesis of magnetic iron oxide nanoparticles using inedible Cynometra ramiflora fruit extract waste and their photocatalytic degradation of methylene blue dye. *Mater. Res. Bull.* **2018**, *97*, 121–127.
52. Vasantharaj S, Sathiyavimal S, Senthilkumar P, LewisOscar F, Pugazhendhi, A. Biosynthesis of iron oxide nanoparticles using leaf extract of Ruellia tuberosa: Antimicrobial properties and their applications in photocatalytic degradation. *J. Photochem. Photobiol. B: Biol.* **2019**, *192*, 74–82.
53. Anchan S, Pai S, Sridevi H, Varadavenkatesan T, Vinayagam R, Selvaraj, R. Biogenic synthesis of ferric oxide nanoparticles using the leaf extract of Peltophorum pterocarpum and their catalytic dye degradation potential. *Biocatal. Agric. Biotechnol.* **2019**, *20*, 101251.
54. Ashraf I, Singh NB, Agarwal A. Green synthesis of iron oxide nanoparticles using Amla seed for methylene blue dye removal from water. *Mater. Today Proc.* **2023**, *72*, 311–316.